

Comparative Study of Photopolymerized Gel Polymer Electrolytes Obtained via ThiolEne Click Reaction for Li Metal Batteries

*Original*

Comparative Study of Photopolymerized Gel Polymer Electrolytes Obtained via ThiolEne Click Reaction for Li Metal Batteries / Longo, M., Gandolfo, M., Plebani, N.A., Calderon, C.A., Destro, M., Fontana, D., Bodoardo, S., Amici, J.. - In: ENERGY & ENVIRONMENT MATERIALS. - ISSN 2575-0356. - 8:5(2025), pp. 1-11. [10.1002/eem2.70028]

*Availability:*

This version is available at: 11583/3007909 since: 2026-02-23T15:18:44Z

*Publisher:*

John Wiley & Sons

*Published*

DOI:10.1002/eem2.70028


*Terms of use:*

This article is made available under terms and conditions as specified in the corresponding bibliographic description in the repository

*Publisher copyright*

(Article begins on next page)

# Comparative Study of Photopolymerized Gel Polymer Electrolytes Obtained via Thiol-Ene Click Reaction for Li Metal Batteries

Mattia Longo, Matteo Gandolfo, Nuria Abigail Plebani, Cecilia Andrea Calderon, Matteo Destro, Daniela Fontana, Silvia Bodoardo, and Julia Amici\* 

**Gel polymer electrolytes (GPEs) present the best compromise between mechanical and electrochemical properties, as well as an improvement of the cell safety in the framework of Li metal batteries production. However, the polymerization mechanism typically employed relies on the presence of an initiator, and is hindered by oxygen, thus impeding the industrial scale-up of the GPEs production. In this work, an UV-mediated thiol-ene polymerization, employing polyethylene glycol diacrylate (PEGDA) as oligomer, was carried out in a liquid electrolyte solution (1 M LiTFSI in EC/DEC) to obtain a self-standing GPE. A comparative study between two different thiol-containing crosslinkers (trimethylolpropane tris(3-mercaptopropionate) - T3 and pentaerythritol tetrakis(3-mercaptopropionate) - T4) was carried out, studying the effects of the crosslinking environment and the GPE production methods on the cell performances. All the produced GPEs present an excellent room temperature ionic conductivity above  $1 \text{ mS cm}^{-1}$ , as well as a wide electrochemical stability window up to 4.59 V. When cycled at a current density of C/10 for more than 250 cycles, all of the tested cells showed a stable cycling profile and a specific capacity  $>100 \text{ mAh g}^{-1}$ , indicating the suitability of such processes for up-scaling.**

## 1. Introduction


Facing the inevitable depletion of fossil-based fuels and the subsequent increase in interest toward renewable energy production, more powerful and efficient energy storage systems are urgently required.<sup>[1]</sup> As the global energy demand keeps growing, it has become increasingly clear that the currently available energy storage systems, based on the Li-ion

M. Longo, M. Gandolfo, Prof. S. Bodoardo, Prof. J. Amici  
Department of Applied Science and Technology, Politecnico di Torino, C.so  
Duca degli Abruzzi 24, Torino 10129, Italy  
E-mail: [julia.amici@polito.it](mailto:julia.amici@polito.it)

N. A. Plebani  
Facultad de Ciencias Químicas, Universidad Nacional de Córdoba, Ciudad  
Universitaria, Córdoba 5000, Argentina  
Prof. C. A. Calderon

Facultad de Matemática, Astronomía, Física y Computación, Universidad  
Nacional de Córdoba, Ciudad Universitaria, Córdoba 5000, Argentina

Dr. M. Destro, Dr. D. Fontana  
COMAU, Via Rivalta 30, Grugliasco 10095, Italy

 The ORCID identification number(s) for the author(s) of this article can be found under <https://doi.org/10.1002/eem2.70028>.

DOI: 10.1002/eem2.70028

technology, fall short on the practical energy and power density requirements.<sup>[2–4]</sup> One of the possible routes to improve the value of practical energy density without large modifications in the cell structure is to switch the commercially used intercalation anode, based on graphite, with Li metal.<sup>[2]</sup> Li metal presents a set of exciting properties, namely the low molecular weight, extremely high specific capacity ( $3860 \text{ mA g}^{-1}$ ) and one of the lowest electrochemical potentials ( $-3.04$  vs standard hydrogen electrode SHE), which enable batteries with such anode to reach high operating voltages and to double the energy density of Li-ion systems.<sup>[5–9]</sup> Nevertheless, the implementation of Li metal as the anode presents several yet unsolved issues that limit the practical applicability of this material in commercial batteries. During operation, the Li metal surface is prone to continuous dendritic growth, causing unstable cycling, short cell lifetime, capacity fading, and safety concerns due to shortcircuits.<sup>[5,10]</sup> The implementation of solid or quasi-solid electrolytes in Li metal batteries

has been shown to at least mitigate dendritic growth due to unstable solid electrolyte interface (SEI), and thus improve the safety of the systems.<sup>[10–12]</sup> Among the possible solid electrolyte types, gel polymer electrolytes (GPEs) have been extensively investigated, given the good compromise between mechanical and electrochemical properties, as well as the elimination of liquid electrolyte leakage.<sup>[13–16]</sup> Swelling a crosslinked structure in a liquid electrolyte is one of the most common strategies to obtain a GPE, but the obtained gels present unacceptable thermal responses, such as swelling and dissolving with temperature changes.<sup>[17]</sup> UV-mediated photopolymerization, on the other hand, presents a desirable set of characteristics, such as low curing temperature, excellent spatial and temporal control, high energy efficiency, and low environmental impact.<sup>[13,17–19]</sup> Acrylate and methacrylate-based monomers and oligomers have been extensively studied for electrochemical applications due to their low cost and reasonable electrochemical stability.<sup>[13,20,21]</sup> Choi et al. investigated a wide variety of GPEs based on poly(4-hydroxybutyl acrylate) (PHBA) with a room temperature ionic conductivity exceeding  $10^{-3} \text{ S cm}^{-1}$ , an initial Columbic efficiency of 99.69% and discharge capacity of  $212.37 \text{ mAh g}^{-1}$ , while cycling in a Li/GPE/NMC811 full cell.<sup>[22]</sup> Employing ethoxylated trimethylolpropane triacrylate (ETPTA) as the polymer skeleton and a

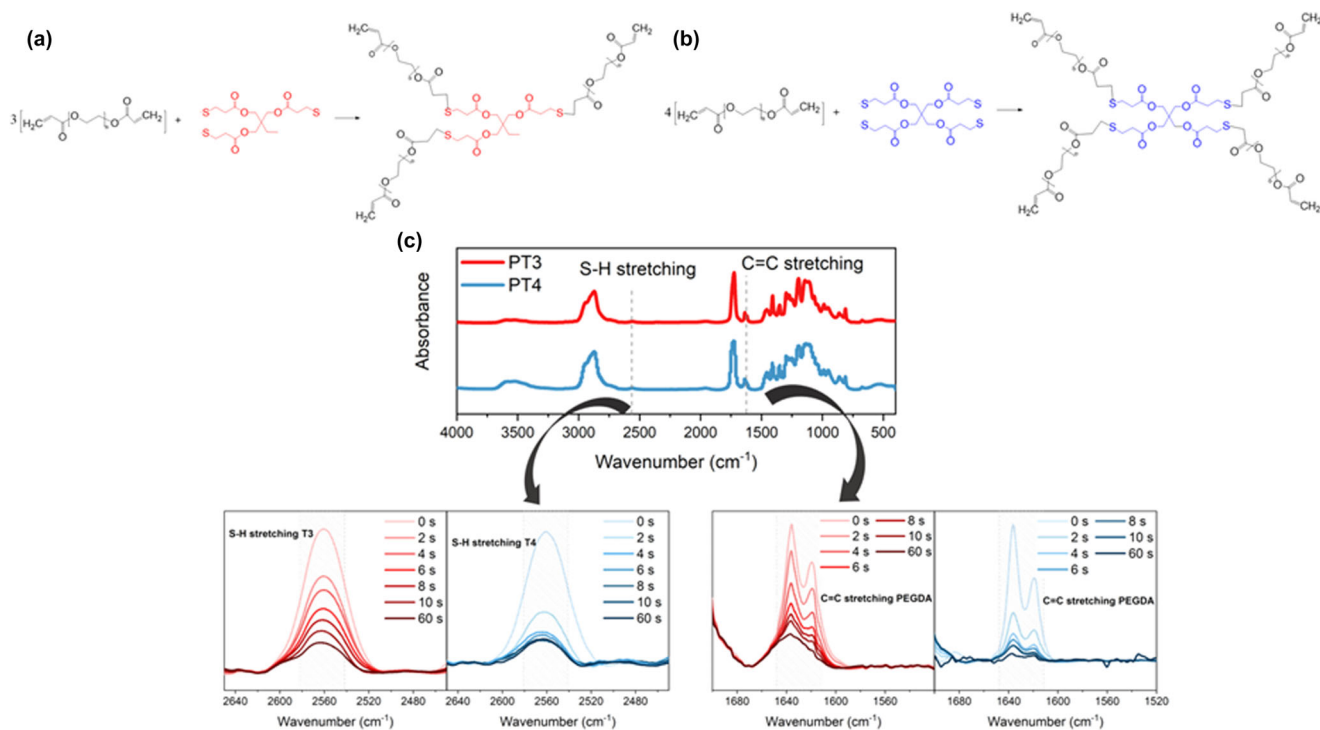
lithium bis(trifluoromethylsulfonyl)-imide (LiTFSI) and tetraglyme solvate ionic liquid as the liquid electrolyte, Gao *et al.* produced a GPE with excellent mechanical and thermal properties and a capacity retention of 99.7% after 750 cycles in a Li/GPE/LiFePO<sub>4</sub> (LFP) at 0.5C.<sup>[23]</sup> Gu *et al.* proposed a non-flammable GPE based on ethoxylated trimethylolpropane triacrylate (ETPTA), fluoroethylene carbonate (FEC), and 1,1,2,2-tetrafluoroethyl 2,2,3,3-tetrafluoropropyl ether (FEPE) cured in the framework of a glass fiber separator (GF) with a high ionic conductivity (1.57 mS cm<sup>-1</sup> at 30 °C) and a capacity retention of 88.4% after 1000 cycles at 2C in a Li/GPE/LFP full cell.<sup>[24]</sup> Nonetheless, the UV-mediated radical polymerization presents a couple of fundamental critical features, that is, the need for a photoinitiator and the high sensitivity toward O<sub>2</sub> presence, rendering the industrial scale up of such systems highly problematic.<sup>[18]</sup> In this optic, the thiol-ene polymerization is regarded as a possible method to overcome these problems. The thiol-ene polymerization results from the reaction between a C=C double bond of an acrylate or methacrylate group and a S-H group of a thiol.<sup>[25]</sup> This reaction is reported to be extremely fast (click reaction), easily obtainable, insensitive to O<sub>2</sub> presence and highly efficient. Additionally, the initiation step does not require a photoinitiator and the obtained gel presents minimal residual stresses and low shrinkage with respect to other polymerization techniques.<sup>[17,25–27]</sup> This work proposes a systematic study toward the up-scalability of the photopolymerization process where different parameters are considered. First, the photocuring of polyethylene glycol diacrylate (PEGDA) is carried out with two different thiol-containing molecules: trimethylolpropane tris(3-mercaptopropionate) (T3) and pentaerythritol tetrakis(3-mercaptopropionate) (T4), in the presence of a carbonate-based liquid electrolyte, obtaining membranes referred to as PT3 and PT4, respectively. Second, the influence of the curing atmosphere is indagated by comparing the properties of membranes cured in an inert Ar-filled glovebox and those prepared in a dry room, to assess the influence of possible water traces on the GPEs crosslinking reaction. Two different production strategies are also implemented, the first one preparing self-standing GPEs and sandwiching them between anode and cathode (referred to as EX), and the second one curing the GPE directly on top of the cathode (referred to as IN). PT3 and PT4 exhibit similar features in the presence or absence of oxygen, with high room temperature ionic conductivity above 10<sup>-3</sup> S cm<sup>-2</sup> and a broad electrochemical stability window up to 4.59 V. However, in general, the PT4 GPE demonstrates higher mechanical and Li transport properties, correlated also to a more homogeneous SEI layer, studied through XPS analysis. Moreover, electrochemical testing on GPEs crosslinked in a dry room demonstrated superior transport properties and overall performances with respect to the glovebox crosslinked ones. Besides, the influence of the IN or EX situ preparation was investigated through a rate capability test in Li/GPE/LFP cells. All the tested cells displayed a stable cycling profile and a specific capacity higher than 100 mAh g<sup>-1</sup> when cycled at a current density of C/10 for more than 250 cycles, demonstrating the suitability of such processes for up-scaling.

## 2. Results

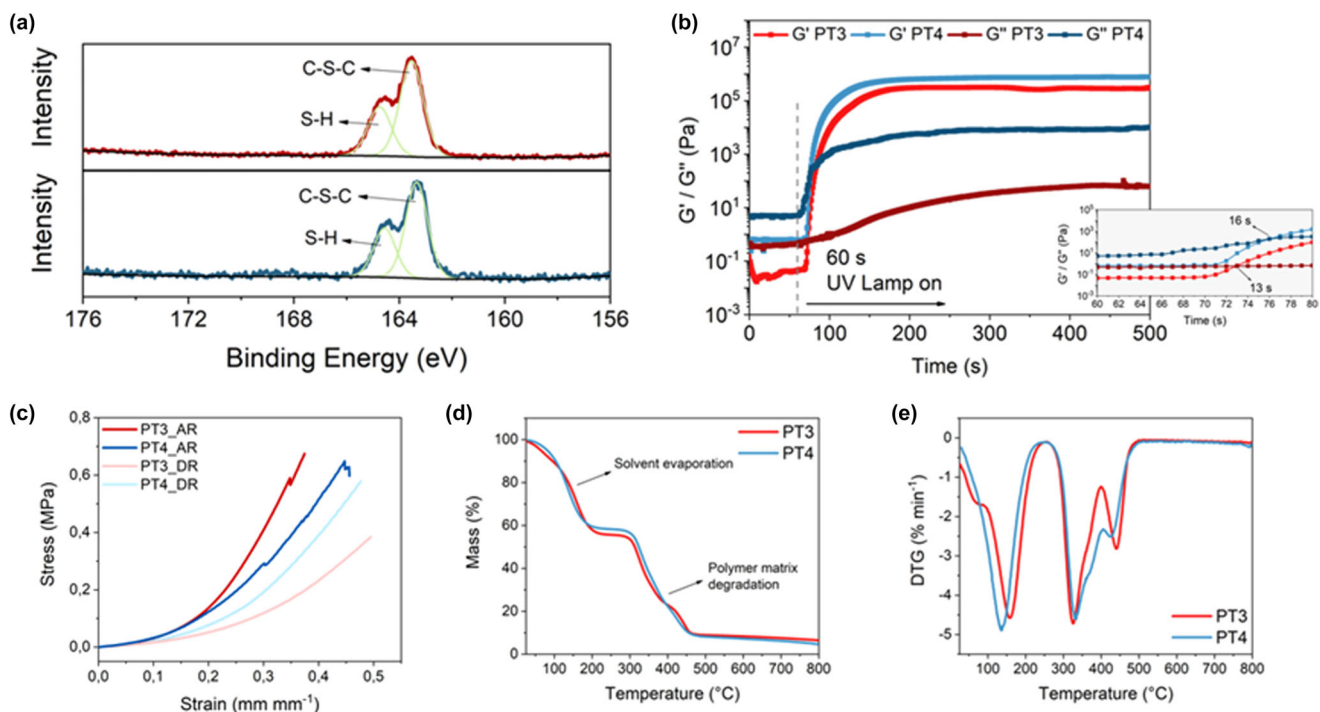
### 2.1. Physico-Chemical Characterization

Figure 1a,b show a schematic representation of the thiol-ene photoinduced click reaction between PEGDA and both crosslinkers T3 and T4. The photopolymerization of the formulations was investigated by

means of FT-IR spectroscopy. The normalized spectra of the precursor solutions are reported in Figure 1c. The curing process was monitored following the decrease of intensity of two characteristic peaks, namely the one at 1640 cm<sup>-1</sup>, relative to the C=C double bond stretching of the PEGDA chains, and the one at 2565 cm<sup>-1</sup>, relative to the S-H bond stretching of T3 and T4 molecules.<sup>[28,29]</sup> The inserts in Figure 1c report the intensity of both peaks during increasing UV irradiation time, demonstrating an intensity decrease of an overall 90% after 60 s of continuous UV irradiation. Conversions were computed as the ratio of the final and the initial integral area of the considered peak and the results are reported in Table S1, Supporting Information. From the obtained FT-IR spectra, it was possible to assess the faster polymerization kinetics of the PT4 formulation, demonstrated by the rapid decrease in intensity in the S-H absorption peak, possibly caused by the higher thiol group density, compared to the PT3 formulation. Such conversions were confirmed by the decrease of intensity of the Raman peaks of the thiol group at 2565 cm<sup>-1</sup> after UV irradiation<sup>[30]</sup> reported in Figure S1, Supporting Information. The higher absolute intensity of the 2565 cm<sup>-1</sup> Raman peak of the PT4 after 1 min of irradiation with UV light could be associated with the lower conversion of thiol groups in the PT4 formulation compared to the PT3 one.<sup>[13]</sup> This could indicate a faster start of the polymerization, which resulted in the rapid generation of a rigid crosslinked structure in the first seconds, reducing the mobility of the remaining S-H moieties and hindering their further reactions with the acrylate groups. The lower availability of S-H groups could also lead to a higher degree of homopolymerization of the PEGDA chains which resulted in the higher conversion of C=C bonds for the PT4 formulation reported in Table S1, Supporting Information. To confirm the lower thiol conversion, an XPS measurement was performed on crosslinked and thoroughly dried PT3 and PT4 membranes. The LiTFSI salt was not added in the precursor solution in order to exclude the presence of peaks relative to the TFSI<sup>-</sup> in the S 2p XPS spectra. The obtained deconvoluted spectra are reported in Figure 2a and the ratio between the integral intensity of the free thiol SH at 164.6 eV peak and the thioether C-S-C peak at 163.1 eV was computed, demonstrating an SH/CSC ratio of 0.535 for the PT3 formulation and 0.555 for the PT4,<sup>[31–33]</sup> thus confirming the lower SH conversion in the PT4 sample. The kinetics of the curing process of the GPEs was further investigated by means of photorheometric analysis with the storage modulus curves as a function of the irradiation time reported in Figure 2b. The PT4 formulation presented a steeper slope, thus confirming the higher polymerization rate and higher reactivity with respect to the PT3 sample.<sup>[34]</sup> As for the final value of storage modulus, the PT3 formulation reached a stable storage modulus value of 0.32 MPa after 135 s, while the PT4 solution reached a value of about 0.75 MPa after 235 s. Such increase in the storage modulus value from PT3 to PT4 was considered to be in accordance with results from the literature.<sup>[27]</sup> The longer time required to reach a stable storage modulus value, together with the higher gel time for PT4 (namely 16 s), could be regarded as a confirmation of the slower reaction kinetics after the creation of the initial crosslinked structure. The increment in the mechanical properties of the obtained GPEs with the increase of thiol functionalities was shown by the compression mechanical testing performed on GPEs crosslinked under Ar atmosphere (AR) and in dry room (DR). Figure 2c shows the stress-strain curves for the two formulations. The obtained values of compression modulus, namely 0.31 MPa for the PT3\_AR sample and 0.34 MPa for the PT4\_AR one, are to be expected due to the higher total crosslink density of the tetrafunctional thiol-based formulation. Nonetheless, the higher modulus can be related to the larger degree of



**Figure 1.** Schematic representation of the thiol-ene reaction between PEGDA and a) T3 and b) T4. c) FTIR spectra of the precursor formulation of PT3 and PT4. Inserts: Intensity decrease of the C=C and the S-H peaks for PT3 and PT4 during UV irradiation.



**Figure 2.** a) S 2p XPS spectra of PT3 (top) and PT4 (bottom) dried membranes, b) photorheometric curves of the samples. Insert: gelation times of the formulations, c) stress-strain curves for samples cured in glovebox (AR) and in dry room (DR), d) thermograms, and e) DTG curves of cured membranes.

homopolymerization of PEGDA in the PT4 formulation, which resulted in a lower presence of the more flexible thiol-ether crosslinks.<sup>[35,36]</sup> The same compression test was carried out on samples photopolymerized in a dry room. These samples displayed much lower values of compression modulus, of the order of 0.15 MPa for PT3\_DR and 0.23 MPa for PT4\_DR. The large difference in the mechanical properties of the samples produced in the dry room can be ascribed to the presence of trace amounts of water, adsorbing from the dry room atmosphere into the formulation, acting as a plasticizer and reducing the modulus of the GPEs.<sup>[37–39]</sup> To assess the presence of water, FTIR spectra were collected of membranes cured both in the dry room and in the Ar-filled glovebox. For each formulation, the normalized spectra of the Ar-cured membranes were subtracted from the spectra of the dry room-cured ones, in order to isolate the water contribution. In Figure S2, Supporting Information such difference is shown. The peaks at around  $1640\text{ cm}^{-1}$  and the wide band at around  $3400\text{ cm}^{-1}$  were attributed to O-H bending and stretching vibrations, respectively.<sup>[40]</sup> The presence of water traces was confirmed in both formulations crosslinked in the dry room. Precursors and GPEs thermal stabilities were investigated via TGA. The thermograms of the PEGDA, T3 and T4 monomers, as well as the cured PT3 and PT4 membranes are reported in Figure 2d and Figure S3a, Supporting Information. PEGDA showed one degradation step at  $320\text{ }^{\circ}\text{C}$  and a residual mass at  $800\text{ }^{\circ}\text{C}$  of about 2.4%, while both T3 and T4 degradation onset was localized at  $225\text{ }^{\circ}\text{C}$ . The cured membranes showed the same thermal degradation steps, losing approximately 50% of the initial weight due to solvent (EC and DEC) evaporation starting at about  $50\text{ }^{\circ}\text{C}$ , followed by the thermal degradation of the residual polymeric matrix at about  $300\text{ }^{\circ}\text{C}$ . From the DTG curves, reported in Figure 2e and Figure S3b, Supporting Information, it was possible to discriminate between three different weight loss steps. The first and most relevant one was associated with the EC and DEC evaporation while the second one, with the highest degradation rate at  $330\text{ }^{\circ}\text{C}$ , was linked to the breakage of the crosslinking S-C bonds and the subsequent generation of char and volatilization of S and C containing species. The third and smallest weight loss step is attributed to the further degradation of the char at around  $430\text{ }^{\circ}\text{C}$ .<sup>[41]</sup> The morphologies of the two membranes were investigated to evaluate the possible presence of porosity developed due to solvent evaporation during the crosslinking reaction. However, micrographs of the PT3 and PT4 surfaces, reported in Figure S4, Supporting Information, present a non-macroporous structure, excluding the possibility of solvent evaporation during UV curing.

## 2.2. Electrochemical Characterization

PT3 and PT4 formulations were crosslinked both in an Ar-filled glovebox and in dry room and tested in coin-type cells in order to evaluate the possible differences in the GPEs electrochemical properties. The ionic conductivity ( $\sigma$ ) measurements were carried out in symmetrical SS/GPE/SS cells through EIS analysis in the temperature range between  $20$  and  $60\text{ }^{\circ}\text{C}$ . Figure 3a reports the  $\sigma$  values for the PT3 and PT4 samples cured both in Ar and in dry room, computed with Equation 1. The linear trends shown in the plot can be regarded as proof that the principal conduction mechanism is to be ascribed to the decoupled ionic diffusion in the liquid phase, as expected from a GPE. However, additional minor conduction mechanisms can be considered responsible for the differences in ionic conductivity of the different GPEs.<sup>[42]</sup> The formulations cured in dry room presented a higher ionic

conductivity than the Ar-cured ones, through the entire temperature range. This effect could be caused by the presence of trace amounts of water acting as a plasticizer thus increasing the chain mobility, as already hypothesized, and the conductivity.<sup>[43,44]</sup> The presence of water traces, however, did not result in the decomposition of the Li salt, as LiTFSI is reportedly stable during water exposure.<sup>[45,46]</sup> The higher PT4 conductivity, both for Ar and dry room-cured GPEs, was likely due to the lower thiol group conversion in the reaction between PEGDA and T4. The greater presence of unbound side chains can increase the segmental motion of the polymer matrix, further increasing mobility, and thus, the ionic conductivity.<sup>[14,35,47]</sup> Another possible effect was the increase in lithium salt dissociation mediated by the greater density of C=O and unreacted S-H group that can interact and partially coordinate the TFSI<sup>-</sup> anions.<sup>[48]</sup> Nonetheless, all tested membranes presented excellent ionic conductivity values, reported in Table S2, Supporting Information. The portion of the total ionic conductivity ascribed to Li<sup>+</sup> movement was computed with the transference number measurement of symmetric Li/GPE/Li cells, applying Equation 2. An higher transference number is preferred as it results in lower polarization at the electrode/electrolyte interface as well as a more homogeneous Li plating. In Figure 3b the average values of the  $t_{\text{Li}^+}$  are reported. The individual chronoamperometry plots for each cell are reported in Figure S5, Supporting Information. The  $t_{\text{Li}^+}$  values displayed the same trend of the ionic conductivity, with the PT4\_DR cell presenting the highest average  $t_{\text{Li}^+}$  value of 0.30 and the PT3\_AR cell presenting the lowest value of 0.24. In order to further understand the Li<sup>+</sup> chemical environment and solvation structure, FTIR spectra were collected comparing the different membranes configurations. Figure S6a, Supporting Information displays the FTIR spectra of membranes crosslinked in the absence and presence of the liquid electrolyte solution. The peak around  $1730\text{ cm}^{-1}$  can be associated to the stretching of the carbonyl group present in the structure of PEGDA and both thiols crosslinkers.<sup>[49]</sup> Adding the EC/DEC solution, two peaks appear at  $1772\text{ cm}^{-1}$  and  $1798\text{ cm}^{-1}$  (reported in Figure S6b, Supporting Information), with the latter associated to the stretching of the carbonyl group of EC and the former to the Fermi resonance of the stretching vibration mode.<sup>[50]</sup> The DEC carbonyl stretching peak is centered around  $1730\text{ cm}^{-1}$  and overlaps with the previously detected peak, thus it was not possible to evaluate. From literature, it is already known that the signal relative to the EC–Li coordination overlaps with the Fermi resonance peak of EC at  $1772\text{ cm}^{-1}$ , hence rendering the deconvolution of this contribution not possible.<sup>[50]</sup> However, it is possible to assess the increase in intensity of the  $1772\text{ cm}^{-1}$  peak, due to the presence of EC–Li coordination. Figure S6c, Supporting Information, on the other hand, displays the ring breathing peak of EC, centered at around  $892\text{ cm}^{-1}$ .<sup>[51]</sup> When comparing these peaks for formulations crosslinked without LiTFSI, a slight blueshift was observed in the case of PT4. This shift, although small, possibly stems from an increased interaction of the EC carbonyl group with the free polymeric moieties containing the polar SH group. The spectra of the membranes containing LiTFSI display a more pronounced blueshift and the appearance of a shoulder at  $902\text{ cm}^{-1}$ , related to the EC–Li interaction.<sup>[51,52]</sup> The PT3\_AR membrane displays higher intensity of the shoulder peak with respect to the PT4\_AR, demonstrating a stronger interaction between EC and Li<sup>+</sup>. This feature could stem from the stronger interactions between PEGDA ethylene oxide (EO) portions and Li<sup>+</sup>, with respect to the EC–Li interactions, demonstrated by higher donor number values found in literature.<sup>[52]</sup> The greater influence of the interactions between PEGDA and Li<sup>+</sup> in the PT4\_AR membrane, possibly due to an increased homopolymerization,

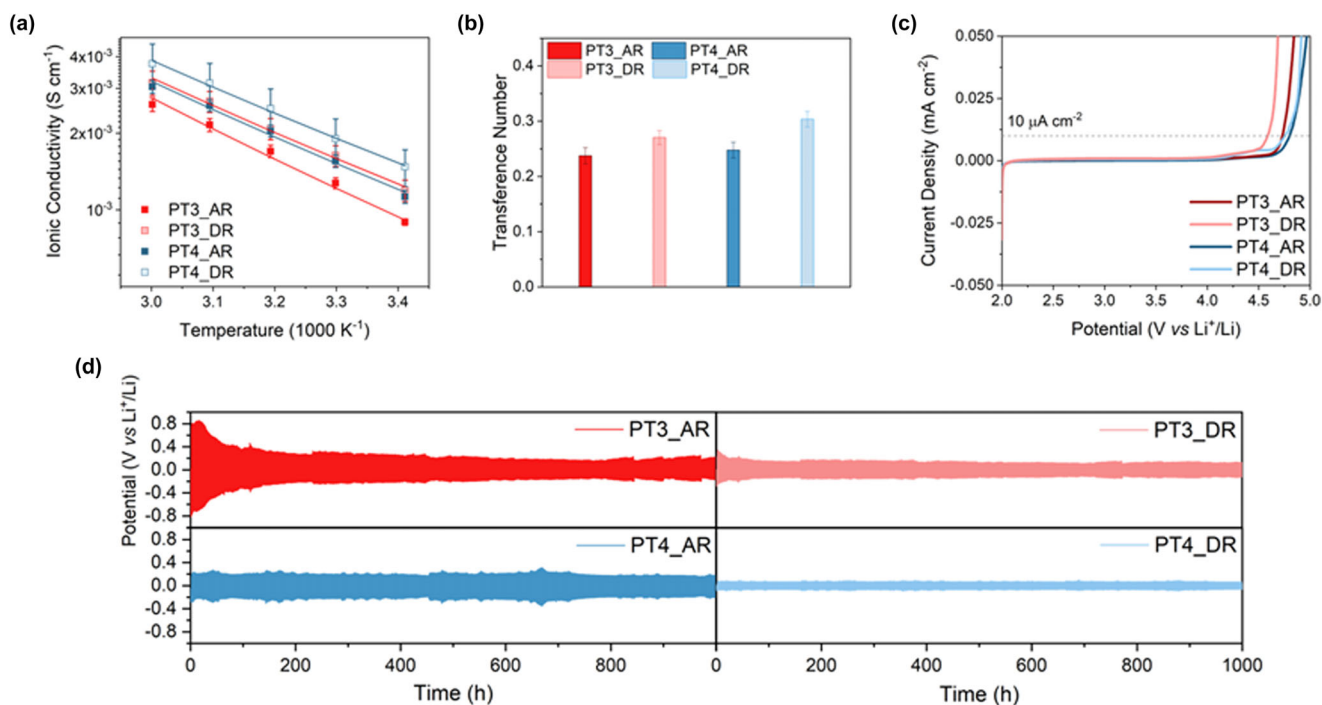


**Figure 3.** a) Arrhenius plot of the formulations, b) AVERAGE transference number of GPEs, c) LSV curves of GPEs, and d) stripping and plating profiles of GPEs.

could also lead to greater LiTFSI dissociation and thus to higher  $t_{Li^+}$  values. In the case of PT3\_DR and PT4\_DR, the same trend is shown, with slightly higher intensities at  $902\text{ cm}^{-1}$  and  $1772\text{ cm}^{-1}$ , and thus slightly stronger EC–Li interaction strengths. This effect, however, is quite small and it is compensated by the increase in ionic conductivity due to improved chain mobility, thus is not appreciable in the  $t_{Li^+}$  values. To assess the electrochemical stability window (ESW) of the different GPEs, a LSV analysis was performed on Li/GPE/SS half cells in the voltage range between 2 and 5 V. The ESW parameter is of great importance to guarantee the operational safety of the GPEs, as an oxidative stability voltage higher than the cutoff voltage is needed to ensure that no degradation reactions occur during cycling. The plot, reported in Figure 3c, shows a good oxidation resistance of the GPEs in contact with Li, with an ESW that extends up to 4.59 V, exceeding the operational voltage range of 4.2 V of the proposed electrochemical system. Another fundamental property for the correct functioning of an electrolyte in a Li metal battery is the long-term stability against Li metal. The evaluation was performed with EIS measurements conducted daily on a symmetric Li/GPE/Li cell kept at OCV for 1 month. The Nyquist plots relative to the different formulations are reported in Figure S7, Supporting Information. As for the cells sporting the membranes cured in the Ar atmosphere, no significant variations in the bulk resistance ( $R_b$ ) or charge transfer resistance ( $R_{ct}$ ) values were observed. For both the PT3\_AR and the PT4\_AR, the  $R_b$  was consistently found equal to  $35\ \Omega$ , while the  $R_{ct}$  value was around  $260\ \Omega$ , demonstrating a good stability against Li metal. The dry room cured membranes displayed lower  $R_b$  values, nominally around  $28\ \Omega$  for the PT3\_DR and  $12\ \Omega$  for the PT4\_DR, reported in Figure S8, Supporting Information, consistent with the higher conductivity associated to the dry room crosslinked GPEs, and a slightly higher  $R_{ct}$  around  $320\ \Omega$  at the end of the considered time. These slightly higher values might be explained by an initial

reaction between metallic lithium and the trace water among other factors. Such values, however, were already stable after 10 days for PT3\_DR and 20 days for PT4\_DR, showing no further evolution of the phenomena afterward. The reversibility of  $Li^+$  transport through the GPEs, as well as the overpotential associated with Li deposition and stripping was investigated by means of a galvanostatic plating and stripping test carried out on symmetric Li/GPE/Li cell with a current density of  $0.1\text{ mA cm}^{-2}$  and a limited specific capacity of  $0.1\text{ mAh cm}^{-2}$ . All the formulations presented a stable voltage profile, reaching 1000 h of cycling with a low overpotential. As shown in Figure 3d, the cells containing PT4 membranes displayed an overpotential of 205.5 and 60.7 mV versus  $Li^+/Li$  after 1000 h, for the PT4\_AR and PT4\_DR formulations, respectively; while the PT3\_AR and PT3\_DR cells reached 1000 h of cycling sporting a higher overpotential of 215.7 and 125.2 mV versus  $Li^+/Li$ , respectively. The lower overpotentials of the PT4 formulations, as well as the increase in cycling stability, was again to be ascribed to their higher ionic conductivity and transport properties. Moreover, focusing on the voltage profile (Figure S9, Supporting Information), all the formulations displayed a significant dead lithium generation on the surface of the electrodes, demonstrated by the arch-like shape of the overpotential in each cycle.<sup>[53,54]</sup> Both the PT4-based formulations, however, displayed smaller slope of such potential arch, and therefore, a more homogeneous  $Li^+$  deposition on the electrodes resulting in a minor dead lithium deposition on the surface. Furthermore, the higher initial overpotential associated to both PT3 cells can be ascribed to the greater presence of free C=C double bonds reacting with Li metal to form a SEI layer. Nonetheless, all tested membranes were able to cycle without major instabilities for 1000 h, retaining a small overpotential, and so can be regarded as stable in contact with metallic lithium and employable as GPEs for Li metal batteries. In order to confirm the superior electrochemical properties of the

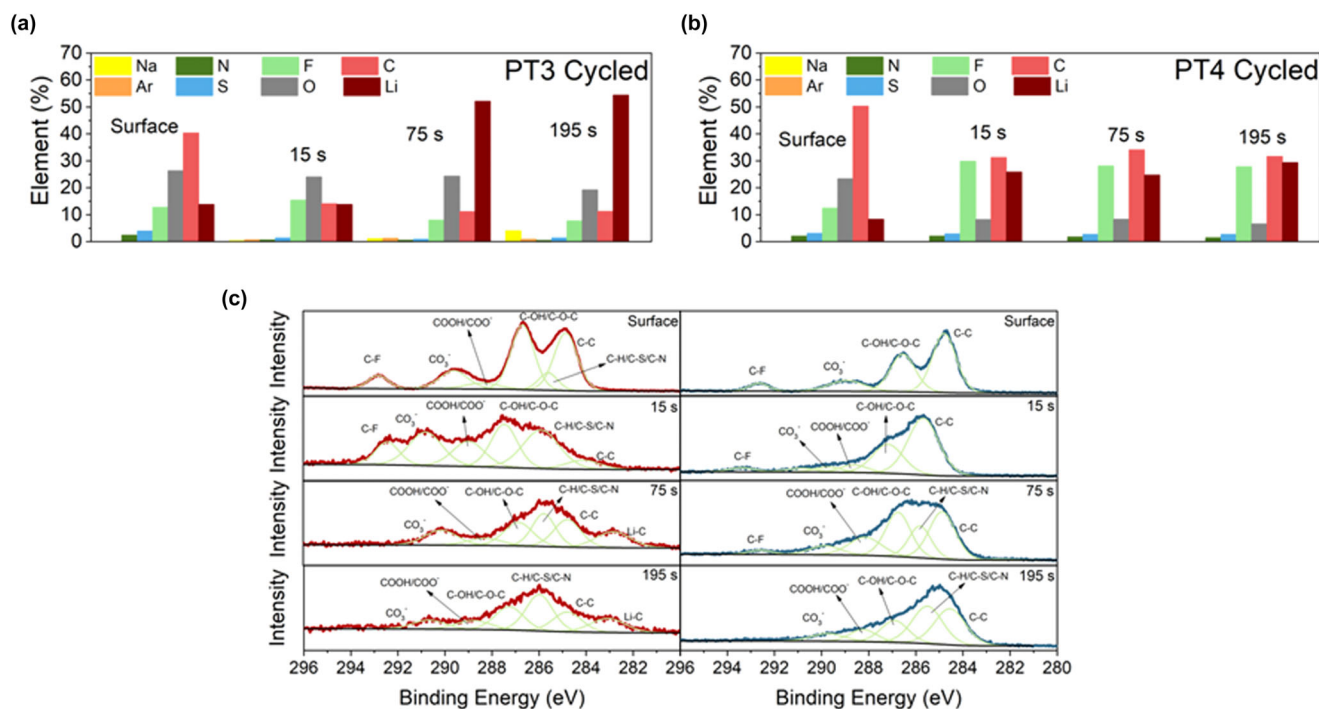


**Figure 4.** Elemental composition of SEI on Li anodes of a) PT3 and b) PT4 cells. c) In depth C 1s spectra on Li metal anode after 10 cycles at C/10 (left PT3 cell, right PT4 cell).

PT4-based membranes, as well as to assess the effect of the crosslinker (T3 and T4) on the SEI formation, symmetric Li/GPE/Li cells were assembled in glovebox and the electrodes surfaces were analyzed after 24 h of rest at OCV and after 10 cycles with a current density of  $0.1 \text{ mA cm}^{-2}$  and a limited capacity of  $0.1 \text{ mAh cm}^{-2}$ , via SEM, EDS, and XPS. Figure S10, Supporting Information shows the Li metal anode surfaces for rested and cycled cells containing the PT3 and PT4 membranes. For reference, Figure S11, Supporting Information shows the surface of a pristine Li metal anode. The Li surfaces of the rested cells presented a similar surface morphology to the pristine Li anode, while the PT3 cycled Li exhibited an irregular surface morphology with pits, cracks, and ridges. The PT4 cycled Li surface was significantly flatter and more homogeneous than the PT3 one but displayed some pits due to the loss of Li metal generating the SEI and dead lithium.<sup>[55]</sup> Concurrently, the Li surfaces were analyzed by means of energy dispersive spectroscopy (EDS) in order to quantify the atomic species. The results of the EDS analysis are reported in Table S3, Supporting Information and clearly showed a higher F percentage in the PT4 rested and cycled cells. Both the F and the S content on the surfaces increases with cycling, possibly due to SEI formation and electrolyte degradation. The S presence was already found to be beneficial in the formation and stabilization processes of the SEI layer.<sup>[56–58]</sup> Interestingly, it was observed that the SEI layer formed on the Li anodes of the PT3 cells, both after the initial rest at OCV and after 10 cycles, was richer in S than the PT4 cells. One possible explanation is the higher proportion of unreacted C=C bonds in PT3, acting as a weak point promoting degradation of the polymer membrane. The lower amount of S on the surface, compared to F, was confirmed by XPS measurements of the atomic composition of the SEI of cycled cells. Figure 4a,b show the atomic percentages of the species present on the surface and in the bulk of the SEI layer. Considering the greater presence of elemental Li on the PT3

cycled anode, it was possible to assume the lower thickness of the transition layer between the electrolyte and the native oxide layer on the Li metal surface. Furthermore, the PT4 transition layer displayed a greater presence of S, N and F, resulting from greater TFSI<sup>-</sup> degradation. This result is in line with the assumption of a superior ionic dissociation of the Li salt in the PT4 membrane due to unreacted thiol groups, as well as the greater presence of C=O groups in the T4 structure. In-depth XPS was performed on the surface of Li anodes extracted from Li/GPE/LFP after 10 cycles of charge and discharge at a current density of  $0.1 \text{ mA cm}^{-2}$ . The spectra, reported in Figure 4c and Figures S12–S15, Supporting Information, were collected at different Ar sputtering times in order to investigate the composition of the transition layer at different depths and thus its history of formation. The main peaks found in the C 1s spectra of Li anodes from both PT3 and PT4 containing cells, at 292.8, 289.6, 286.7, and 284.9 eV, were assigned to C-F, possibly TFSI<sup>-</sup> residuals,  $\text{Li}_2\text{CO}_3$ , C-O and C-C groups, respectively.<sup>[24,59]</sup> Interestingly in the PT4 spectra, the intensities of peaks relative to organic species (C-O, C=O, C-H and C-C) decreased in the bulk of the SEI, with the inorganic  $\text{Li}_2\text{CO}_3$  peak intensity presenting a less significant decrease. Considering the O 1s spectra, the same trend was reported, with peaks relative to inorganic species such as the peak at 531.9 eV, assigned to  $\text{Li}_2\text{CO}_3$ , being more intense in the bulk, and peaks relative to organic ones, such as the one at 533.6 eV assigned to C=O, being more intense on the surface.<sup>[56,60]</sup> In the bulk of the SEI layer of the PT3 sample, the peak at 528.5 eV of the O 1s spectra, assigned to  $\text{Li}_2\text{O}$ , and at 161.7 and 160.5 eV of the S 2p spectra, assigned to  $\text{Li}_2\text{S}$ , are significant and are either absent or present with a lower intensity in the bulk PT4 spectra.<sup>[56,60,61]</sup> The presence of  $\text{Li}_2\text{O}$  in both samples was also confirmed in the Li 1s spectra, due to the presence of the peak centered around 54.3 eV, with a lower intensity for the PT4.<sup>[59–61]</sup> These results were in accordance with the

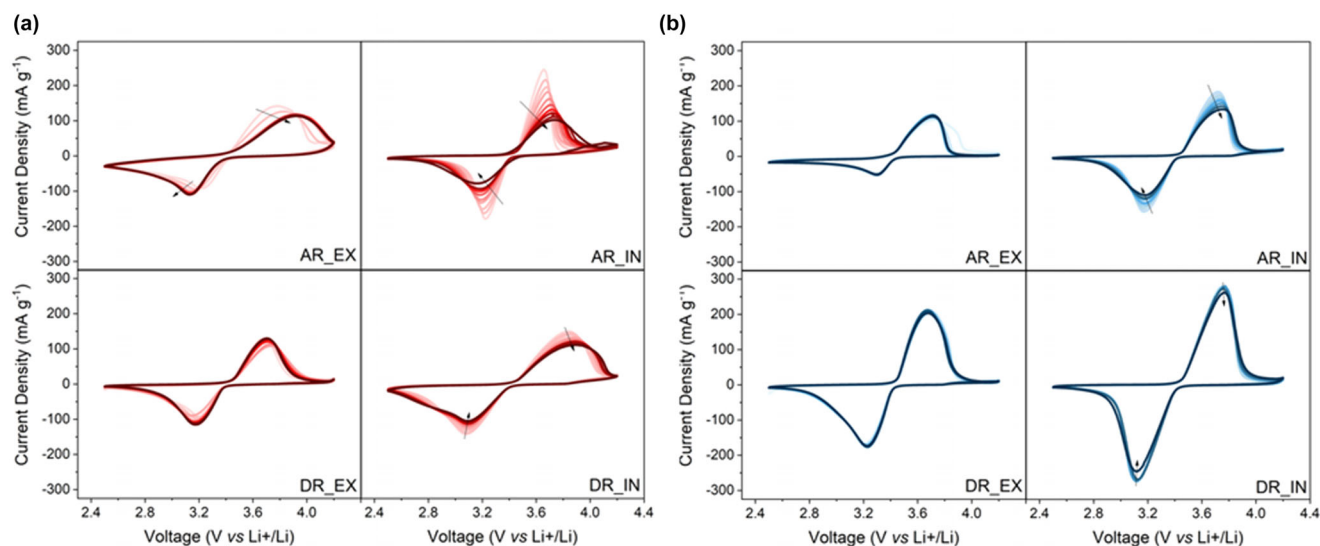


**Figure 5.** Cyclic voltammetry profiles of a) PT3 and b) PT4 cells cycled at a rate of  $0.1 \text{ mV s}^{-1}$ .

assumption that the Li anodes of PT4 cells displayed a thicker but more homogeneous transition layer. Further proof of this hypothesis lied in the presence of peaks at 52.9 eV in the PT3 Li 1s and 283.1 eV in the PT3 C 1s spectra, assigned to Li metal and C-Li, which are not present in the PT4 spectra.<sup>[59,62]</sup> The presence of such peaks can be correlated with an inhomogeneous transition layer, exposing the native oxide layer thus enabling greater electrolyte decomposition.<sup>[63]</sup> Furthermore, the F 1s and the Li 1s spectra displayed peaks at 684.7 and 56.8 eV respectively, which were linked to the presence of LiF, mainly in the transition layer.<sup>[64,65]</sup> The lower relative intensities of  $\text{Li}_2\text{CO}_3$  (Figure 4c) and LiF (Figure S14, Supporting Information) peaks in the bulk of the transition layer of PT4 cells was directly linked to the lower decomposition of the electrolyte, which confirmed the superior Li surface protection due to the thicker transition layer.<sup>[63]</sup> The presence of LiF in both SEIs is still to be considered a positive aspect due to the extra-high mechanical properties, which are beneficial in stopping dendritic growth, as well as correlating with fast  $\text{Li}^+$  transport, SEI stabilization, and improved Columbic efficiency.<sup>[59,64]</sup> The S 2p spectra displayed some characteristic peaks that demonstrated the participation of the TFSI<sup>-</sup> anion and the crosslinkers in the forming reactions of the SEI. The presence of peaks assigned to  $\text{SO}_4^-$ , TFSI<sup>-</sup> and its degraded products was more significant on the surface of the tested anodes, while the contribution of  $\text{Li}_2\text{S}$ , S-S, and di- and poly-sulfides increased in the bulk.<sup>[31,56,61]</sup> The last investigated parameter was the GPE precursors' deposition process and its influence on cells performances. Cyclic voltammetry tests were performed to evaluate possible differences in electrochemical stability due to the different crosslinking environments and deposition methods. **Figure 5a,b** display the CV curves of all the considered formulations in the potential range between 2.5 and 4.2 V. Table S4, Supporting Information reports the potentials of the anodic and cathodic peaks as well as the polarization potential for each formulation. PT4 formulations showed limited polarization after 10 cycles, as well as comparatively higher intensities of both the anodic and cathodic peaks, consistent with the superior conductivity and  $t_{\text{Li}^+}$ .<sup>[65]</sup> Comparing PT3 and PT4 membranes for each different production method, it was possible to notice the higher selectivity and efficiency of the electrochemical reactions in the PT4 formulations, shown

by more centered peaks and higher current intensities. Li/GPE/LFP cells were prepared in the glovebox and cycled for 10 cycles at a current density of C/10 to investigate the impact of the different formulations and production methods on the cathode morphology and surface composition by SEM. In the case of in situ cells, the morphology of the cathode presented significant differences between cycled (Figure S16, Supporting Information) and pristine conditions, as shown in Figure S17, Supporting Information, due to the presence of GPE residues after cell disassembly. For PT3 cells, the amount of degradation products on the surface after 10 cycles at C/10, was arguably greater than PT4 cells, demonstrating lower electrochemical stability. A rate capability test was conducted on Li/GPE/LFP cells aiming at determining the electrochemical performances of the GPEs at different C-rates. The cells were cycled between 2.5 and 4.2 V at C/20, C/10, C/5, C/2, and 1C for 5 cycles before 10 cycles at C/10 and the results are reported in **Figure 6a**. Tested cells showed good capacity values, higher than  $100 \text{ mAh g}^{-1}$  at C/10 with an almost total capacity retention after 5 cycles at 1C. The PT3 cells presented, on average, higher specific capacities than the PT4 cells and a larger data dispersion with an overall unstable Columbic efficiency, possibly caused by a significant degradation of the GPEs during cycling. **Figure 6b** displays the voltage profiles of cells cycled at C/10 before and after the rate capability test. All tested cell configurations presented a good reversibility of the charge and discharge voltage profile with a significant capacity retention. The lower polarization displayed by PT4 cells further confirmed the superior ionic conductivity and transport properties of this formulation. Considering the long cycling test, the higher stability of the PT4 cells was confirmed considering the capacity fade values reported in Table S5, Supporting Information, as well as the flatter and more stable capacity profile, shown in **Figure 7a–d**. Almost all tested cells displayed a capacity fade lower than 10% after more than 250 cycles, with the PT4 formulations consistently demonstrating a superior capacity retention and cycling stability than the PT3. Moreover, tested in situ PT4 cells presented comparable lifetime and specific capacity value to other in situ GPEs, with a superior capacity retention during cycling (Figure 7e).<sup>[66–72]</sup> In the cases of PT3\_AR\_EX the lower capacity fade was caused by the continuous degradation of the electrolyte and the significantly unstable cycling,

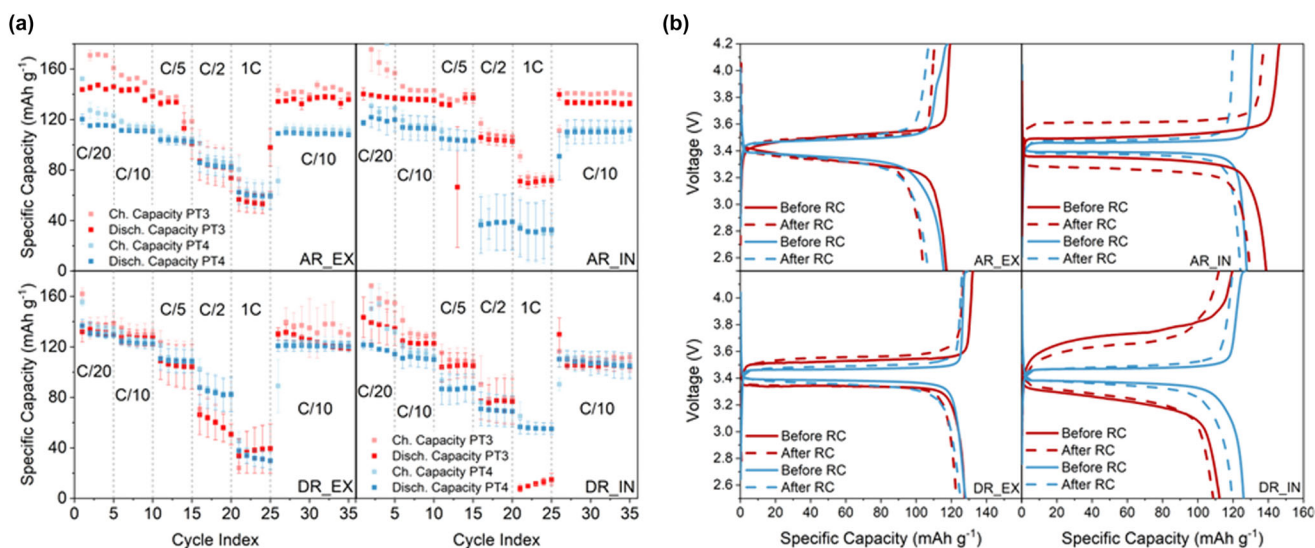


**Figure 6.** a) Rate capability test of GPEs for all configurations, b) Voltage profile at a current density of C/10 before and after a rate capability test (red PT3 cell, blue PT4 cell).

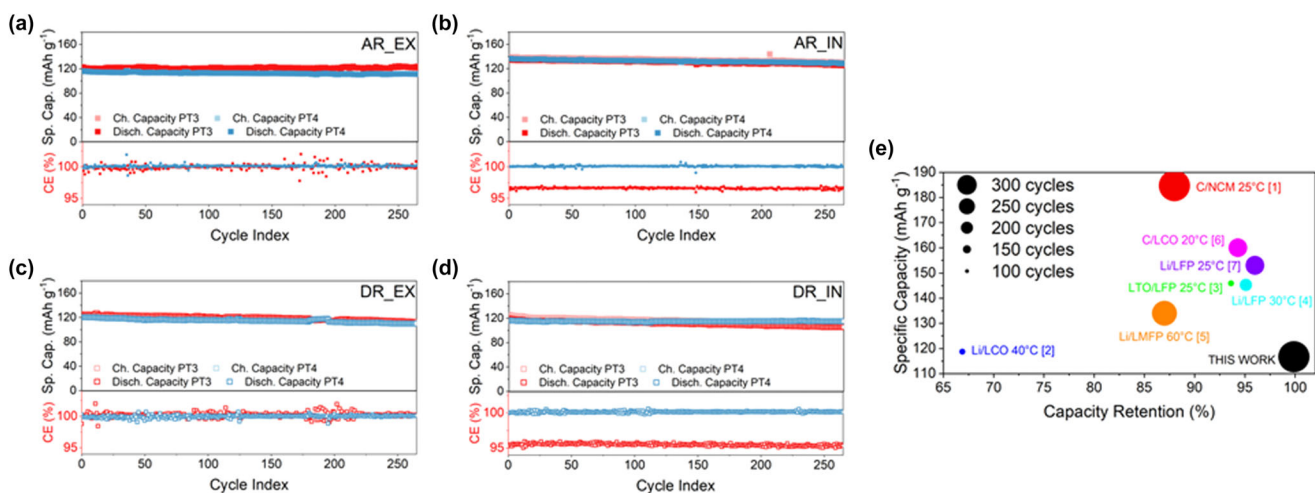


**Figure 7.** Long cycling capacity evolution and Columbic efficiency for GPEs in a) AR\_EX, b) AR\_IN, c) DR\_EX, and d) DR\_IN configurations, e) Comparison between specific capacity, capacity retention after cycling and lifetime of PT4\_DR\_IN with in situ crosslinked GPEs.

which was not demonstrated in the respective PT4 plot. Comparing the properties of ex situ and in situ membranes, a significant increase in the long cycling specific capacity of the cell was found, stemming from the improved contact between the GPEs and the cathodes. The increase of the capacity was more significant for the PT4 formulations as the ex situ membrane presented higher mechanical properties than the PT3\_EX one, which possibly worsen its electrochemical performances. Interestingly, the in situ deposited PT3 formulations displayed a lower Columbic efficiency than the PT4 ones, possibly due to the onset of parasitic reactions occurring at the cathode interface during the charge process. The more disperse Columbic efficiency, higher than 100%, associated to the PT3\_EX cells was possibly related to the less homogeneous SEI formed, continuously exposing fresh Li metal during cycling. On the other hand, the low Columbic efficiency demonstrated by the

PT3\_IN cells could stem from a loss of contact as well as the onset of parasitic reactions due to a non-complete polymerization in the cathode porosities during the curing process. Furthermore, the continuous reaction of Li metal with the PT3 electrolytes to reform the SEI layer was possibly responsible for the larger capacity fade for the PT3 cells.

### 3. Conclusion

A comparative study was conducted studying the physico-chemical and electrochemical properties of a class of GPEs based on PEGDA575 and a thiol-containing crosslinker, obtained in different production environments. A thorough investigation was carried out by FTIR, Raman, XPS, and photorheometry, in order to investigate the polymerization reaction

and its relationship to the electrochemical properties. The obtained GPEs displayed excellent ionic conductivity higher than  $1 \text{ mS cm}^{-1}$ , as well as good transport properties and stability in contact with the Li metal electrodes. The dry room curing was found to not compromise the polymerization reaction, but instead to improve the ionic conductivity and the electrochemical performances overall, due to the beneficial effect on the chain mobility and the salt ionic dissociation. The rate capability tests demonstrated an almost complete capacity retention after cycling at 1C, with a C/10 capacity higher than  $100 \text{ mAh g}^{-1}$  for all cells. The in situ deposited membranes presented comparable electrochemical properties with respect to the ex situ membranes, displaying a contained capacity fade after more than 250 cycles, thus demonstrating suitable properties for application in Li-ion battery systems. The production strategies displayed in this work can be considered a suitable approach to the development of cheap, green, and easily up-scalable gel polymer electrolytes for future Li metal systems.

#### 4. Experimental Section

**Materials:** Poly(ethylene glycol) diacrylate (PEGDA,  $M_n = 575 \text{ g mol}^{-1}$ ), trimethylolpropane tris(3-mercaptopropionate) (T3,  $M_n = 398.56 \text{ g mol}^{-1}$ ), pentaerythritol tetrakis(3-mercaptopropionate) (T4,  $M_n = 488.66 \text{ g mol}^{-1}$ ), ethylene carbonate (EC,  $M_n = 88.06 \text{ g mol}^{-1}$ ), diethyl carbonate (DEC,  $M_n = 118.13 \text{ g mol}^{-1}$ ), lithium bis(trifluoromethanesulfonyl)imide (LiTFSI,  $M_n = 287.1 \text{ g mol}^{-1}$ ), lithium iron (II) phosphate (LFP,  $M_n = 157.76 \text{ g mol}^{-1}$ ), 1-methyl-2-pyrrolidone (NMP,  $M_n = 99.13 \text{ g mol}^{-1}$ ), poly(vinylidene fluoride) (PVDF, 8% solution in NMP), and carbon black (C65) were obtained from Sigma-Aldrich and used without further purification.

**GPE production:** The precursor PT3 solution was prepared by mixing in a glass vial 0.170 g of PEGDA, 0.039 g of T3, and 0.490 g of LiTFSI 1 M in EC/DEC 1:1 v/v in an Ar-filled glovebox (Mbraun Labstar, Stratham, NH, USA,  $\text{O}_2$  and  $\text{H}_2\text{O}$  contents <0.5 ppm). The PT4 precursor solution was similarly prepared by mixing 0.173 g of PEGDA, 0.037 g of T4, and 0.490 g of the liquid electrolyte solution. The oligomer concentration was kept at 30% wt for the two formulations. The precursor solutions were stirred for 10 min until thoroughly mixed and completely clear, and then cast onto a glass plate and irradiated with UV light (Hamamatsu UV LightningCure LC8 L9588, Hamamatsu, Shizuoka, Japan) for 1 min until a self-standing gel was obtained. To evaluate the possible differences between the properties of the membranes, the same precursor solutions were also prepared in a dry room, and the photopolymerization was carried out in a dry atmosphere (10% relative humidity, dew point  $20^\circ\text{C}$ ). To discriminate between the two production methods, the membranes obtained in a controlled Ar atmosphere were named PT3\_AR and PT4\_AR, while the membranes produced in the dry room were referred to as PT3\_DR and PT4\_DR. The self-standing membranes were cut into disks with an 18 mm diameter and an average thickness of  $300 \mu\text{m}$ . Throughout the article, the acronym GPE will refer indifferently to PT3\_AR, PT3\_DR, PT4\_AR, or PT4\_DR, the common point being a polymer matrix crosslinked around the liquid electrolyte solution.

**LFP cathode production:** To prepare the cathode, a slurry containing 70% LFP, 20% C65, and 10% PVDF wt% in NMP was cast onto an aluminum foil and dried in the oven at  $50^\circ\text{C}$  for 1 h. Disks with a 15 mm diameter were cut and further dried in a vacuum oven (Glass Oven B-585, Büchi, Uster, Switzerland) at  $120^\circ\text{C}$  for 6 h. The active material mass loading of the obtained cathodes was  $\approx 2 \text{ mg cm}^{-2}$ .

**Cell assembly:** The cell assembly was carried out in the glovebox for the PT3\_AR and PT4\_AR cells and in the dry room for the PT3\_DR and PT4\_DR ones. Lithium chips ( $15.6 \text{ mm} \times 0.62 \text{ mm}$ , Chemetall s.r.l., Giussano, Italy) were employed as the anode while an LFP electrode was employed as the cathode. The full cells were assembled by sandwiching the self-standing membranes between the lithium chip and the LFP cathode. This cell configuration was referred to as EX. For the in situ cured membranes, the precursor solution was directly deposited on the cathode and irradiated with UV light for 1 min until completely polymerized. The cells containing the in situ polymerized GPEs were referred to as IN.

**Physico-chemical characterization:** The polymerization of the oligomers was investigated via FT-IR spectroscopy employing a ThermoFischer Scientific FT-IR Spectrometer (Thermo Scientific, Waltham, USA) in a wavenumber range between  $525$  and  $2200 \text{ cm}^{-1}$  with 32 scans and a resolution of  $4 \text{ cm}^{-1}$  in ambient air. Raman spectra were collected in the interval between  $400$  and  $3500 \text{ cm}^{-1}$  with a Reinschaw InVia instrument (Raman, Wotton-under-Edge, UK) employing a laser wavelength of  $514 \text{ nm}$  and a  $20\times$  lens. The thermal resistance of the oligomers and the membranes was explored by means of a thermogravimetric analysis (TGA) with a Netzsch thermo-microbalance (TG 209 F3 Tarsus, Selb, Germany) between  $25$  and  $800^\circ\text{C}$  in an inert  $\text{N}_2$  atmosphere with a rate of  $20^\circ\text{C min}^{-1}$ . The polymerization kinetics was studied by monitoring the storage modulus of the cured gels with an Anton PAAR Modular Compact Rheometer (Physica MCR 302, Graz, Austria) sporting a quartz bottom glass during UV irradiation with a Hamamatsu UV LightningCure LC8 L9588 UV lamp. The gel time was computed as the time for which the storage modulus  $G'$  surpasses the loss modulus  $G''$ . Mechanical compression testing was performed by an MTS Systems Corporation dynamometer (MTS QTestTM/10 Elite, Eden Prairie, MN, USA) with a  $10 \text{ N}$  load cell and a  $1\text{-mm min}^{-1}$  compression rate. The compression modulus was computed as the slope of the initial elastic region. The GPEs morphology was obtained by means of a Field Emission Scanning Electron Microscope (FESEM, ZEISS Supra 40, Oberkochen, Germany). X-Ray Photoelectron Spectroscopy (XPS) measurements were carried out on Li anodes and crosslinked membranes with a ThermoScientific K-Alpha X-ray Photoelectron Spectrometer (Thermo Scientific, Waltham, USA) employing a non-monochromatized Al-K excitation radiation. The electrodes morphology before and after 10 cycles of galvanostatic cycling was obtained with Field Emission Scanning Electron Microscope (FESEM, ZEISS Sigma, Oberkochen, Germany), equipped with an Energy Dispersive X-Ray Spectroscopy detector.

**Electrochemical characterization:** Electrochemical impedance spectroscopy (EIS) was employed in order to probe the ionic conductivity of the membranes. The EIS measurements were performed by a VSP3-e multichannel potentiostat (Biologic, Seyssinet-Pariset, France) in the frequency range between  $1 \text{ Hz}$  and  $10^5 \text{ Hz}$  at open circuit voltage (OCV) with an amplitude of  $0.01 \text{ V}$ . The measurements were carried out in the temperature range between  $20$  and  $60^\circ\text{C}$  in a dynamic climatic chamber (BINDER GmbH, Tuttlingen, Germany) employing a stainless-steel SS/GPE/SS symmetrical cell configuration (ECC-Std, EL-Cell, GmbH, Hamburg, Germany). The values of the ionic conductivities were computed by the equation:

$$\sigma = \frac{s}{R_b \cdot A} \quad (1)$$

where  $\sigma$  is the ionic conductivity,  $s$  and  $A$  are respectively the GPE thickness and area and  $R_b$  is the bulk resistance of the membranes computed from the intercept of the high-frequency Nyquist plot of the EIS measurement. The long-term interfacial stability of the GPEs in contact with Li metal was investigated by means of EIS measurements performed each day for a month on symmetrical Li/GPE/Li cells kept at room temperature. The  $\text{Li}^+$  transference number ( $t_{\text{Li}^+}$ ) of the GPEs was computed from EIS measurements performed before and after a chronoamperometry on a symmetrical Li/GPE/Li cell. The voltage step was  $10 \text{ mV}$  over the OCV and the value of  $t_{\text{Li}^+}$  was computed by the following:

$$t_{\text{Li}^+} = \frac{I_s \cdot (\Delta V - I_0 R_0)}{I_0 \cdot (\Delta V - I_s R_s)} \quad (2)$$

where  $I_s$  and  $I_0$  are the steady state and initial currents,  $R_s$  and  $R_0$  are the steady state and initial interfacial resistances and  $\Delta V$  is the voltage step. The electrochemical stability of the GPE was investigated by means of a linear sweep voltammetry (LSV) performed on SS/GPE/Li half cells in the voltage range between  $2$  and  $5 \text{ V}$  versus  $\text{Li/Li}^+$  with a scan rate of  $0.1 \text{ mV s}^{-1}$  employing a CHI660D Electrochemical Workstation (CH Instruments, Inc, Austin, TX, USA). The cyclic voltammetry (CV) was carried out on full Li/GPE/LFP cells by a VSP3-e multichannel potentiostat in the voltage range between  $2.5$  and  $4.2 \text{ V}$  versus  $\text{Li/Li}^+$  with a scan rate of  $0.1 \text{ mV s}^{-1}$ . A BT-2000 battery tester (Arbin Instruments, College Station, USA) was employed to carry out the galvanostatic cycling tests on full Li/GPE/LFP cells between  $2.5$  and  $4.2 \text{ V}$ , as well as the plating and stripping tests on

symmetrical Li/GPE/Li cells with a current density of 0.1 mA cm<sup>-2</sup> and a limited capacity of 0.1 mAh cm<sup>-2</sup>.

## Acknowledgements

The authors want to thank Prof. Marco Armandi for his valuable contributions in the data interpretation and Dr. Mattia Spedicati for the possibility to perform mechanical testing. This publication is part of the project PNRR-NGEU, which has received funding from the MUR-DM 352/2022. Open access publishing facilitated by Politecnico di Torino, as part of the Wiley - CRUI-CARE agreement.

## Conflict of Interest

The authors declare no conflict of interest.

## Supporting Information

Supporting Information is available from the Wiley Online Library or from the author.

## Keywords

gel polymer electrolytes, in situ depositions, Li metal anodes, thiol-ene polymerizations, up-scalability

Received: October 29, 2024

Revised: April 6, 2025

Published online: April 10, 2025

- [1] F. Arshad, J. Lin, N. Manurkar, E. Fan, A. Ahmad, M. u. N. Tariq, F. Wu, R. Chen, L. Li, *Resour. Conserv. Recycl.* **2022**, *180*, 106164.
- [2] S. M. George, S. Sampath, A. J. Bhattacharyya, *Batter. Supercaps* **2022**, *5*, e202200252.
- [3] Y. K. Liu, C. Z. Zhao, J. Du, X. Q. Zhang, A. B. Chen, Q. Zhang, *Small* **2023**, *19*, e2205315.
- [4] J. Xu, X. Cai, S. Cai, Y. Shao, C. Hu, S. Lu, S. Ding, *Energy Environ. Mater.* **2023**, *6*, e12450.
- [5] J. Wang, B. Ge, H. Li, M. Yang, J. Wang, D. Liu, C. Fernandez, X. Chen, Q. Peng, *Chem. Eng. J.* **2021**, *420*, 129739.
- [6] J. Xiao, Q. Li, Y. Bi, M. Cai, B. Dunn, T. Glossmann, J. Liu, T. Osaka, R. Sugiura, B. Wu, J. Yang, J. G. Zhang, M. S. Whittingham, *Nat. Energy* **2020**, *5*, 561.
- [7] X. Xiong, W. Yan, Y. Zhu, L. Liu, L. Fu, Y. Chen, N. Yu, Y. Wu, B. Wang, R. Xiao, *Adv. Energy Mater.* **2022**, *12*, 2103112.
- [8] B. Peng, Z. Liu, Q. Zhou, X. Xiong, S. Xia, X. Yuan, F. Wang, K. I. Ozoemena, L. Liu, L. Fu, Y. Wu, *Adv. Mater.* **2024**, *36*, e2307142.
- [9] S. Park, R. Chaudhary, S. A. Han, H. Qutaish, J. Moon, M. S. Park, J. H. Kim, *Energy Mater.* **2023**, *3*, 300005.
- [10] J. Li, Y. Cai, H. Wu, Z. Yu, X. Yan, Q. Zhang, T. Z. Gao, K. Liu, X. Jia, Z. Bao, *Adv. Energy Mater.* **2021**, *11*, 2003239.
- [11] Z. Wang, J. Chen, J. Fu, Z. Li, X. Guo, *Energy Mater.* **2024**, *4*, 400050.
- [12] Q. Zhou, X. Yang, X. Xiong, Q. Zhang, B. Peng, Y. Chen, Z. Wang, L. Fu, Y. Wu, *Adv. Energy Mater.* **2022**, *12*, 2201991.
- [13] M. H. Ryou, Y. M. Lee, K. Y. Cho, G. B. Han, J. N. Lee, D. J. Lee, J. W. Choi, J. K. Park, *Electrochim. Acta* **2012**, *60*, 23.
- [14] R. L. Weber, M. K. Mahanthappa, *Soft Matter* **2017**, *13*, 7633.
- [15] M. C. Long, G. Wu, X. L. Wang, Y. Z. Wang, *Energy Storage Mater.* **2022**, *53*, 62.
- [16] J. Li, H. Fu, M. Gu, J. Chen, J. Zhou, L. Fan, B. Lu, *Nano Lett.* **2024**, *24*, 11419.
- [17] E. A. Baroncini, J. F. Stanzone, *Int. J. Biol. Macromol.* **2018**, *113*, 1041.
- [18] A. Lewandowska, P. Gajewski, K. Szcześniak, M. Sadej, P. Patelski, A. Marcinkowska, *Polymers* **2021**, *13*(3), 1.
- [19] C. Xuan, S. Gao, Y. Wang, Q. You, X. Liu, J. Liu, R. Xu, K. Yang, S. Cheng, Z. Liu, Q. Guo, *J. Power Sources* **2020**, *456*, 228024.
- [20] V. Jabbari, V. Yurkiv, M. G. Rasul, M. T. Saray, R. Rojaee, F. Mashayek, R. Shahbazian-Yassar, *Energy Storage Mater.* **2022**, *46*, 352.
- [21] J. Amici, C. A. Calderón, D. Versaci, G. Luque, D. Barraco, E. Leiva, C. Francia, S. Bodoardo, *Electrochim. Acta* **2022**, *404*, 139772.
- [22] H. J. Choi, Y. J. Jeong, H. S. Choi, J. S. Kim, J. Ahn, W. Shin, B. M. Jung, E. Cho, H. J. Lee, J. H. Choi, M. J. Choi, J. Yoon, J. W. Yi, G. T. Hwang, J. K. Yoo, K. Chung, *Chem. Eng. J.* **2023**, *474*, 145673.
- [23] X. Gao, W. Yuan, Y. Yang, Y. Wu, C. Wang, X. Wu, X. Zhang, Y. Yuan, Y. Tang, Y. Chen, C. Yang, B. Zhao, *ACS Appl. Mater. Interfaces* **2022**, *14*, 43397.
- [24] Y. Gu, L. Yang, S. Luo, E. Zhao, N. Saito, *Ionics* **2022**, *28*, 3743.
- [25] C. E. Hoyle, C. N. Bowman, *Angew. Chem. Int. Ed.* **2010**, *49*, 1540.
- [26] C. Piedrahita, V. Kusuma, H. B. Nulwala, T. Kyu, *Solid State Ionics* **2018**, *322*, 61.
- [27] B.-S. Chiou, R. J. English, S. A. Khan, *Macromolecules* **1996**, *29*, 5368.
- [28] A. Beyler-Çiğil, H. Birtane, F. Şen, M. V. Kahraman, *Mater Today Commun.* **2021**, *27*, 102463.
- [29] S. Narute, T. Kyu, *Solid State Ionics* **2022**, *385*, 116010.
- [30] P. Bazylewski, R. Divigalpitaya, G. Fanchini, *RSC Adv.* **2017**, *7*, 2964.
- [31] K. Chen, J. Liu, X. Zhang, Y. Sun, H. Xie, *J. Colloid Interface Sci.* **2024**, *669*, 529.
- [32] J. Cao, Y. Zuo, H. Lu, Y. Yang, S. Feng, *J. Photochem. Photobiol. A Chem.* **2018**, *350*, 152.
- [33] D. G. Castner, K. Hinds, D. W. Grainger, *Langmuir* **1996**, *12*, 5083.
- [34] J. Wang, S. Stanic, A. A. Altun, M. Schwentenwein, K. Dietliker, L. Jin, J. Stampfl, S. Baudis, R. Liska, H. Grützmacher, *Chem. Commun.* **2018**, *54*, 920.
- [35] N. B. Cramer, C. N. Bowman, *J. Polym. Sci. A Polym. Chem.* **2001**, *39*, 3311.
- [36] J. Ahn, Y. Lee, J. Kim, S. Yoon, Y. C. Jeong, K. Y. Cho, *Polymer* **2022**, *250*, 124898.
- [37] Z. L. Goh, N. K. Farhana, F. Kamarulazam, M. Pershaana, S. Bashir, K. Ramesh, S. Ramesh, *Macromol. Rapid Commun.* **2025**, *46*, e2400481.
- [38] Y. N. Sudhakar, M. Selvakumar, D. K. Bhat, *Mater. Sci. Eng. B* **2014**, *180*, 12.
- [39] V. Mazzini, G. Liu, V. S. J. Craig, *J. Chem. Phys.* **2018**, *148*, 222805.
- [40] X. Guo, L. Liu, J. Wu, J. Fan, Y. Wu, *RSC Adv.* **2018**, *8*, 4214.
- [41] T. Wang, L. Li, Q. Wang, G. Xie, C. Guo, *Ind. Crop. Prod.* **2019**, *141*, 111798.
- [42] A. Mahun, P. Černoch, B. Paruzel, H. Beněš, R. Konefał, E. Hleli, Z. Morávková, T. Kazda, J. Brus, L. Kobera, S. Abbrent, *Solid State Ionics* **2023**, *389*, 116096.
- [43] M. G. Cowan, A. M. Lopez, M. Masuda, Y. Kohno, W. M. McDanel, R. D. Noble, D. L. Gin, *Macromol. Rapid Commun.* **2016**, *37*, 1150.
- [44] G. Foran, D. Mankovsky, N. Verdier, D. Lepage, A. Pré Bé, D. Aymé-Perrot, M. L. Dollé, *iScience* **2020**, *23*, 101597.
- [45] S. F. Lux, L. Terborg, O. Hachmöller, T. Placke, H.-W. Meyer, S. Passerini, M. Winter, S. Nowak, *J. Electrochem. Soc.* **2013**, *160*, A1694.
- [46] D. Reber, R. Figi, R. S. Kühnel, C. Battaglia, *Electrochim. Acta* **2019**, *321*, 134644.
- [47] M. S. Grewal, M. Tanaka, H. Kawakami, *Polymer* **2020**, *186*, 122045.
- [48] G. Lu, Y. Zhang, J. Zhang, X. Du, Z. Lv, J. Du, Z. Zhao, Y. Tang, J. Zhao, G. Cui, *Carbon Energy* **2023**, *5*, e287.
- [49] F. Askari, M. Zandi, P. Shokrolahi, M. H. Tabatabaei, E. Hajirasoliha, *Prog. Biomater.* **2019**, *8*, 169.
- [50] D. M. Seo, S. Reininger, M. Kutcher, K. Redmond, W. B. Euler, B. L. Lucht, *J. Phys. Chem. C* **2015**, *119*, 14038.
- [51] P. Wróbel, P. Kubisiak, A. Eilmel, *J. Phys. Chem. B* **2021**, *125*, 1248.
- [52] C. S. Kim, S. M. Oh, *Electrochim. Acta* **2000**, *45*, 2101.

- [53] K. H. Chen, K. N. Wood, E. Kazyak, W. S. Lepage, A. L. Davis, A. J. Sanchez, N. P. Dasgupta, *J. Mater. Chem. A* **2017**, *5*, 11671.
- [54] X. Liu, X. Xin, L. Shen, Z. Gu, J. Wu, X. Yao, *ACS Appl. Energy Mater.* **2021**, *4*, 3975.
- [55] H. Liu, X. B. Cheng, R. Xu, X. Q. Zhang, C. Yan, J. Q. Huang, Q. Zhang, *Adv. Energy Mater.* **2019**, *9*, 1902254.
- [56] P. Jankowski, N. Lindahl, J. Weidow, W. Wiczonek, P. Johansson, *ACS Appl. Energy Mater.* **2018**, *1*, 2582.
- [57] L. P. Hou, L. Y. Yao, C. X. Bi, J. Xie, B. Q. Li, J. Q. Huang, X. Q. Zhang, *J. Energy Chem.* **2022**, *68*, 300.
- [58] L. Lin, K. Yang, R. Tan, M. Li, S. Fu, T. Liu, H. Chen, F. Pan, *J. Mater. Chem. A* **2017**, *5*, 19364.
- [59] P. Jaumaux, Q. Liu, D. Zhou, X. Xu, T. Wang, Y. Wang, F. Kang, B. Li, G. Wang, *Angew. Chem. Int. Ed.* **2020**, *59*, 9134.
- [60] J. Guo, Z. Wen, M. Wu, J. Jin, Y. Liu, *Electrochem. Commun.* **2015**, *51*, 59.
- [61] R. Grissa, V. Fernandez, N. Fairley, J. Hamon, N. Stephant, J. Rolland, R. Bouchet, M. Lecuyer, M. Deschamps, D. Guyomard, P. Moreau, *ACS Appl. Energy Mater.* **2018**, *1*, 5694.
- [62] K. N. Wood, G. Teeter, *ACS Appl. Energy Mater.* **2018**, *1*, 4493.
- [63] D. Kang, S. Sardar, R. Zhang, H. Noam, J. Chen, L. Ma, W. Liang, C. Shi, J. P. Lemmon, *Energy Storage Mater.* **2020**, *27*, 69.
- [64] W. Li, W. Liu, Z. Cai, B. Huang, H. Zhong, Y. Mai, *J. Energy Storage* **2023**, *68*, 107766.
- [65] X. Ye, W. Xiong, T. Huang, X. Li, Y. Lei, Y. Li, X. Ren, J. Liang, X. Ouyang, Q. Zhang, J. Liu, *Appl. Surf. Sci.* **2021**, *569*, 150899.
- [66] W. Chae, B. Kim, W. S. Ryoo, T. Earmme, *Polymers* **2023**, *15*, 803.
- [67] Z. Yang, Y. Luo, X. Gao, R. Wang, *ChemElectroChem* **2020**, *7*, 2599.
- [68] Q. Wang, X. Xu, B. Hong, M. Bai, J. Li, Z. Zhang, Y. Lai, *Chem. Eng. J.* **2022**, *428*, 131331.
- [69] Q. Liu, B. Cai, S. Li, Q. Yu, F. Lv, F. Kang, Q. Wang, B. Li, *J. Mater. Chem. A* **2020**, *8*, 7197.
- [70] W. K. Shin, J. Cho, A. G. Kannan, Y. S. Lee, D. W. Kim, *Sci. Rep.* **2016**, *6*, 26332.
- [71] H. S. Kim, S. I. Moon, *J. Power Sources* **2005**, *146*, 584.
- [72] H. Xu, W. Ye, Q. Wang, B. Han, J. Wang, C. Wang, Y. Deng, *J. Mater. Chem. A Mater.* **2021**, *9*, 9826.